JOURNAL OF COMPUTATIONAL PHYSICS 51, 139–158 (1983)

An Integral Equation Method for the Solution of Singular Slow Flow Problems

M. A. KELMANSON

Department of Applied Mathematical Studies, University of Leeds, Leeds LS2 9JT, England

Received July 1, 1982; revised November 16, 1982

A biharmonic boundary integral equation method (BBIE) is used to solve a two-dimensional contained viscous flow problem. In order to achieve a greater accuracy than is usually possible in this type of method, analytic expressions are used for the piecewise integration of all of the kernel functions rather than the more time-consuming method of Gaussian quadrature. Because the boundary conditions for the problem under consideration—commonly referred to as the "stick–slip" problem—give rise to a singularity in the solution domain for the biharmonic stream function, we find that the rate of convergence of the solution is poor in the neighbourhood of the singularity. Hence a modified BBIE (MBBIE) method is presented which takes into account the analytic nature of the aforementioned singularity. This modification is seen to produce rapid convergence of the results everywhere. The BBIE and MBBIE also provide information concerning the pressure and velocity fields of the flow and these properties are in excellent agreement with the analytical results of Watson.

1. INTRODUCTION

In recent years the use of integral equations in the numerical solution of elliptic boundary value problems (BVP) has gained in popularity [1–4]. The boundary integral equation method (BIE) has the big advantage over finite difference (FD) and finite element (FE) methods of superior convergence and greatly reduced requirements in computer storage and programming [5].

Integral equation methods have been employed previously in viscous flow problems. In a series of papers, Youngren, Acrivos, and Rallison [6–9] solved for the deformation of a fluid drop under various flow conditions. The Stokes equations were solved in terms of velocities and Stokeslets on the drop surface. Mir–Mohamed–Sadegh and Rajagopal [10] solved the biharmonic equation for the stream function over projections and depressions in a channel, although their approach differed to the present formulation, which has the advantage of automatically providing the fluid vorticity. Black *et al.* [11] described an integral equation method for the solution of the biharmonic equation for the case when the gradient of the stream function is known on the boundary.

0021-9991/83 $3.00

In this paper, we investigate the stream function ψ for slow two-dimensional steady viscous flow which satisfies the biharmonic equation

$$\nabla^4 \psi = 0. \tag{1}$$

Coleman [12] solves this equation using a contour integral formulation (which uses Chebyshev quadrature for the integration of the kernel functions) but reveals that there are limitations to the BVPs to which his method can be applied. However, his formulation easily accommodates problems with boundary conditions on normal stresses. The BBIE formulation presented here may be applied to any linear BVP no matter how complex the boundary geometry may be. To demonstrate the applicability of this method we shall examine the flow in a simple geometry. The problem under consideration is commonly referred to as the "stick–slip" problem and contains a sudden discontinuity in boundary conditions which has the effect of introducing a mathematical singularity into the solution domain. This problem has received much attention [12–14] and we shall present a comparison of results from which we conclude that there is excellent agreement between the results obtained using the MBBIE and those obtained from the Wiener–Hopf technique employed by Watson [13]. Motz [15], Symm [16], and several other authors have investigated mathematically the effects of singularities in elliptic equations and their methods have been employed to solve physical problems in the fields of electrostatics [17] and heat transfer [18]. The effect of singularities in biharmonic problems has been investigated analytically by Richardson [14], and Xanthis *et al.* [19] have considered the singular nature of cracks in fracture mechanics problems using integral equation methods. When singularities arise in viscous flow problems many numerical investigations completely ignore their effects or assume that they affect only the flow in the immediate neighbourhood [12, 20, 21]. The inevitable result of such neglect is to introduce errors into the solution near the singularity. In order to improve the accuracy in this region, we include the analytic form of the singularity in the BBIE, having derived it in the manner described by Michael [22].

The results indicate that the effect of the singularity is most influential on the convergence of the solution in its immediate vicinity and that neglecting the singular behaviour produces results whose accuracy must be treated with caution.

2. BBIE Formulation

In order to solve the biharmonic equation for the stream function ψ in a domain Ω enclosed by a boundary $\partial\Omega$, we define a function ϕ by splitting the biharmonic equation into its coupled form [23].

$$\nabla^2 \psi = \phi, \tag{2}$$

$$\nabla^2 \phi = 0, \tag{3}$$

where ϕ is the fluid vorticity.

We can solve Eqs. (2) and (3) given the equivalent of two boundary conditions at each point of $\partial\Omega$. Invoking Green's Theorem in the plane of Eqs. (2) and (3) and employing arguments analogous to those presented by Fairweather *et al.* [23] give the following expressions at the general field point p:

$$\eta(p)\,\psi(p) = \int_{\partial\Omega} \{\psi(q)\log'|p-q| - \psi'(q)\log|p-q|\}\,d\omega(q)$$

$$+ \tfrac{1}{4}\int_{\partial\Omega} \{\phi(q)\,G'(p,q) - \phi'(q)\,G(p,q)\}\,d\omega(q), \tag{4}$$

$$\eta(p)\,\phi(p) = \int_{\partial\Omega} \{\phi(q)\log'|p-q| - \phi'(q)\log|p-q|\}\,d\omega(q), \tag{5}$$

where

(i) $p \in \Omega + \partial\Omega$, $q \in \partial\Omega$.

(ii) $d\omega(q)$ denotes the differential increment of $\partial\Omega$ at q.

(iii) $G(p,q) = |p-q|^2\{\log|p-q| - 1\}$.

(iv) The prime refers to differentiation with respect to the outward normal to $\partial\Omega$ at q.

(v) $\eta(p)$ is defined by

$$\eta(p) = 0 \qquad \text{if } p \notin \Omega + \partial\Omega,$$

$$= \text{internal angle included between the tangents to } \partial\Omega \text{ on either side of } p \text{ if } p \in \partial\Omega,$$

$$= 2\pi \text{ if } p \in \Omega.$$

In practice the integrals in Eqs. (4) and (5) can rarely be solved analytically, thus some form of numerical approximation is necessary. Following Jaswon and Symm [2] we divide $\partial\Omega$ into N smooth straight-line segments $\partial\Omega j$, $j = 1,\ldots,N$, containing boundary nodes q_j, $j = 1,\ldots,N$. Over each interval $\partial\Omega j$ we approximate ψ, ψ', ϕ, and ϕ' in Eqs. (4) and (5) by piecewise-constant functions ψ_j, ψ_j', ϕ_j, and ϕ_j', $j = 1,\ldots,N$. Applying the corresponding discretized forms of Eqs. (4) and (5) at the midpoint $p \equiv q_i$, $i = 1,\ldots,N$, of each interval gives

$$\eta_i\psi(q_i) = \sum_{j=1}^{N}\Bigg[\psi_j\int_{\partial\Omega j}\log'|q_i-q|\,d\omega(q)$$

$$- \psi_j'\int_{\partial\Omega j}\log|q_i-q|\,d\omega(q) + \tfrac{1}{4}\phi_j\int_{\partial\Omega j}G'(q_i,q)\,d\omega(q)$$

$$- \tfrac{1}{4}\phi_j'\int_{\partial\Omega j}G(q_i,q)\,d\omega(q)\Bigg]. \tag{6}$$

$$\eta_i\phi(q_i) = \sum_{j=1}^{N} \left[\phi_j \int_{\partial\Omega j} \log' |q_i - q| \, d\omega(q) - \phi_j' \int_{\partial\Omega j} \log |q_i - q| \, d\omega(q) \right], \tag{7}$$

where now $q_i \in \partial\Omega$ and $q \in \partial\Omega$. Thus introducing

$$A_{ij} = \int_{q\in\partial\Omega_j} \log' |q_i - q| \, d\omega(q) - \eta_j\delta_{ij}, \tag{8}$$

$$B_{ij} = -\int_{q\in\partial\Omega_j} \log |q_i - q| \, d\omega(q), \tag{9}$$

$$C_{ij} = \tfrac{1}{4} \int_{q\in\partial\Omega_j} \{|q_i - q|^2 \log |q_i - q| - |q_i - q|^2\}' \, d\omega(q), \tag{10}$$

$$D_{ij} = -\tfrac{1}{4} \int_{q\in\partial\Omega_j} \{|q_i - q|^2 \log |q_i - q| - |q_i - q|^2\} \, d\omega(q), \tag{11}$$

where δ_{ij} is the Kronecker delta, enables Eqs. (6) and (7) to reduce to the coupled system of vector equations

$$A\psi + B\psi' + C\phi + D\phi' = 0, \tag{12}$$

$$A\phi + B\phi' = 0, \tag{13}$$

where, for example,

$$(A)_{ij} = A_{ij}, \tag{14}$$

$$\psi = (\psi_1, \ldots, \psi_N)^{\mathrm{T}}. \tag{15}$$

Previous authors [24, 25] evaluate the coefficients C_{ij} and D_{ij} in expressions (10) and (11) using Gaussian quadrature. Unfortunately this inevitably introduces errors and is very time consuming. In this paper, these coefficients will be evaluated analytically.

Consider the general field point p in domain Ω surrounded by boundary $\partial\Omega$. Let q_{aj} and q_{bj} be points on $\partial\Omega$ marking the endpoints of boundary segment $\partial\Omega_j$. Then if

$$\begin{aligned} a &= |p - q_{aj}|, \\ b &= |p - q_{bj}|, \\ h &= |q_{aj} - q_{bj}|, \\ \beta &= \angle q_{bj} q_{aj} p, \\ \zeta &= \angle q_{aj} p q_{bj}, \end{aligned} \tag{16}$$

we have the geometry as shown in Fig. 1. Notice here that if p lies in the immediate neighbourhood of $\partial\Omega_j$, but not on $\partial\Omega_j$, then the use of the Gaussian quadrature on expressions (8)–(11) will become computationally expensive, since the integral kernels will become logarithmically singular.

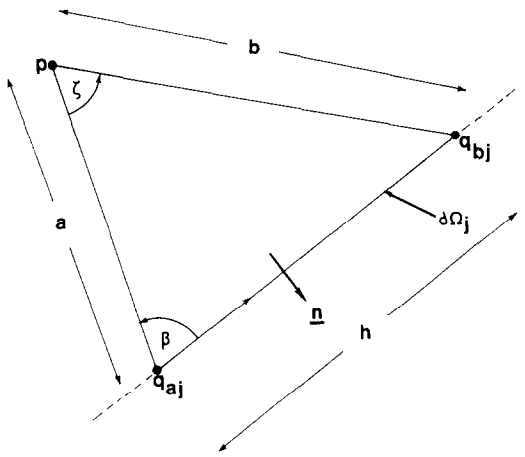

FIG. 1. Notation for analytic evaluation of integrals on straightline segment $\partial\Omega_j$.

Using the notation of relations (16) we have the following analytic expression for the integrals in Eqs. (8)–(11):

$$\int_{\partial\Omega_j} \log' |p-q|\, d\omega = \zeta, \tag{17}$$

$$\int_{\partial\Omega_j} \log |p-q|\, d\omega = a(\log a - \log b)\cos\beta + h\log b - h + a\zeta\sin\beta \equiv I, \text{ say}, \tag{18}$$

$$\int_{\partial\Omega_j} \{|p-q|^2 \log|p-q| - |p-q|^2\}'\, d\omega = a(2I-h)\sin\beta, \tag{19}$$

$$\begin{aligned}\int_{\partial\Omega_j} \{|p-q|^2 \log|p-q| - |p-q|^2\}\, d\omega &= \tfrac{1}{3}\{(h-a\cos\beta)^3(\log b - \tfrac{4}{3}) + (a\cos\beta)^3(\log a - \tfrac{4}{3})\} \\ &\quad + (a\sin\beta)^2\{I - \tfrac{2}{3}h - \tfrac{1}{3}a\zeta\sin\beta\}.\end{aligned} \tag{20}$$

Thus a source of error inherent in previously presented BBIEs has been removed by the introduction of expressions (19) and (20). Expressions (17)–(20) provide us with all the matrix coefficients in Eqs. (12) and (13), and since the problem is biharmonic we need the equivalent of two boundary conditions on each boundary segment $\partial\Omega_j$. In the problem currently considered any two of ψ_j, ψ_j', ϕ_j and ϕ_j' are known for each $j = 1,\ldots,N$ and we can therefore insert this known information into Eqs. (12) and (13). Having done this we may solve the system of coupled equations by employing a direct matrix inversion scheme to solve for the two unknown boundary conditions on

each $\partial\Omega_j$, $j = 1,..., N$. Note that we can solve for unknown boundary conditions on segment $\partial\Omega_j$ when a linear combination of ψ_j, ψ_j', ϕ_j, and ϕ_j' is known; we do not necessarily require explicit boundary conditions. The inversion scheme used was a Gaussian elemination double precision scheme, which was considered preferable to a Gauss–Seidel or S.O.R. scheme because the matrices generated were very dense, and hence not suitable for iterative methods. At this stage the values of ψ_j, ψ_j', ϕ_j, and ϕ_j' are known for each $j = 1,..., N$. A discretized form of Eqs. (4) and (5) provides ψ and ϕ at a general field point $p \in \Omega + \partial\Omega$, i.e., the stream function and vorticity are generated simultaneously using this formulation.

In the present work the BBIE is modified to incorporate the analytic nature of a singularity which arises in the solution domain. We investigate what is commonly referred to as the "stick–slip" problem which has been studied analytically by Richardson [14] and Watson [13], and numerically by Coleman [12].

We solve for the biharmonic stream function ψ which satisfies

$$\nabla^4 \psi = 0 \tag{21}$$

in the infinite strip $-1 \leqslant y \leqslant +1$. The x and y velocity components for this flow are defined by

$$u = \frac{\partial \psi}{\partial y}, \qquad v = -\frac{\partial \psi}{\partial x}, \tag{22}$$

respectively.

Hence the "stick–slip" boundary conditions for the problem are

$$\psi = \pm 1, \qquad \psi_y = 0 \qquad \text{on } y = \pm 1 \text{ in } x < 0, \tag{23a}$$

$$\psi = \pm 1, \qquad \psi_{yy} = 0 \qquad \text{on } y = \pm 1 \text{ in } x > 0. \tag{23b}$$

All remaining boundary conditions on ψ come from the imposition of a parabolic velocity profile as $x \to -\infty$ and a slug-flow profile as $x \to +\infty$. Since $v \to 0$ as $x \to \pm\infty$, then Eq. (22) allows us to evaluate the corresponding conditions on ψ as $x \to \pm\infty$. Employing a symmetry argument, we need only solve for ψ in the upper half of the channel $0 \leqslant y \leqslant 1$. The velocity profile conditions should, in theory, be applied an infinite distance both upstream and downstream. In practice they were applied at $x = \pm X$ for various values of X. A value of $X = 3$ was found to be sufficiently large; taking $X > 3$ caused no appreciable change in the results presented. This gives the boundary conditons on the region $-3 \leqslant x \leqslant 3$, $0 \leqslant y \leqslant 1$ as follows:

$$\psi = 1, \qquad \psi_y = 0 \qquad \text{on } y = 1, x < 0, \tag{24a}$$

$$\psi = 1, \qquad \psi_{yy} = 0 \qquad \text{on } y = 1, x > 0, \tag{24b}$$

$$\psi = 0, \qquad \psi_{yy} = 0 \qquad \text{on } y = 0, \tag{24c}$$

$$\psi_x = 0, \qquad \psi_y = \tfrac{3}{2}(1 - y^2) \qquad \text{on } x = -3, \tag{24d}$$

$$\psi_x = 0, \qquad \psi_y = 1 \qquad \text{on } x = 3. \tag{24e}$$

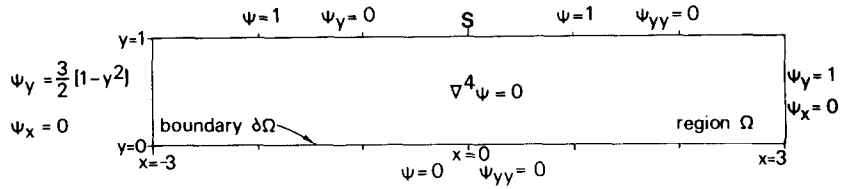

FIG. 2. Solution domain and boundary conditions for the "stick–slip" problem.

The values of ψ_y on $x = \pm 3$ are those which allow unit mass flow in unit time past the "inlet" and "outlet." A pictorial representation of the specified problem is given in Fig. 2 and solution is now facilitated using the BBIE described above.

Boundary discretizations comprising 70, 140, and 280 segments of equal length were used to check convergence of results in the solution domain $\Omega + \partial\Omega$. Convergence was found to be very good except in the vicinity of the point (0, 1) which we subsequently refer to as S. The sudden discontinuity in boundary conditions at $x = 0$ on $y = 1$ gives rise to a mathematical singularity at S. We now incorporate the analytic nature of this singularity into the BBIE to produce a modified BBIE (MBBIE).

It is well known that separated solutions of Eq. (21) in plane polar coordinates (r, θ) are of the form

$$\psi = r^{\lambda+1} f_\lambda(\theta), \tag{25}$$

where λ is a real or complex constant called the exponent of the solution [26], and

$$f_0(\theta) = A\cos\theta + B\sin\theta + C\theta\cos\theta + D\theta\sin\theta, \tag{26a}$$

$$f_1(\theta) = A\cos 2\theta + B\sin 2\theta + C\theta + D, \tag{26b}$$

$$f_\lambda(\theta) = A\cos(\lambda+1)\theta + B\sin(\lambda+1)\theta + C\cos(\lambda-1)\theta + D\sin(\lambda-1)\theta. \tag{26c}$$

If we take polar coordinates centred on S as indicated in Fig. 3, then the constants A, B, C, and D in Eqs. (26) are determined from the four boundary conditions given in Eqs. (24a) and (24b) on $\theta = 0$ and $\theta = \pi$, respectively. It should be noted that the analytic form of the singularity is very much dependent on the local geometry of the

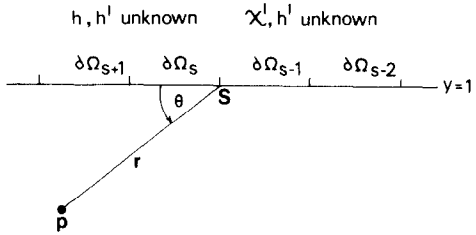

FIG. 3. Boundary discretization and polar coordinates employed near singularity at S.

solution domain. In cases where are no-slip conditions on the boundary of a flow-in-a-corner which encloses an angle of less than 146.3 degrees [27], the exponents in Eq. (25) are all complex. In such cases there is the further complication of first finding these exponents numerically and then extracting only the real part of the solution.

Solutions of Eq. (21) for the present problem are found in the form of Eqs. (25) and (26c). (Solutions dependent on Eqs. (26a) and (26b) arise only when the flow is generated by "moving-boundary" conditions.) The boundary conditions (24a) and (24b) imply that

$$f_\lambda(0) = \frac{df_\lambda}{d\theta}(0) = f_\lambda(\pi) = \frac{d^2 f_\lambda}{d\theta^2}(\pi) = 0. \tag{27}$$

Insertion of conditions (27) into Eq. (26c) gives two possible sets of solutions

$$f_\lambda(\theta) = a_\lambda\{\cos(\lambda+1)\theta - \cos(\lambda-1)\theta\}, \qquad \lambda = \tfrac{1}{2}, \tfrac{3}{2}, \tfrac{5}{2}, \ldots, \tag{28}$$

or

$$f_\lambda(\theta) = b_\lambda\{(\lambda-1)\sin(\lambda+1)\theta - (\lambda+1)\sin(\lambda-1)\theta\}, \qquad \lambda = 2, 3, 4, \ldots, \tag{29}$$

where a_λ and b_λ are arbitrary constants.

Since $\psi = 1$ at point S, then using the linearity of the problem we have

$$\psi(r,\theta) = 1 + \sum_{k=1}^{\infty} \beta_k r^{\lambda_k+1} f_{\lambda_k}(\theta), \tag{30}$$

where now the constants A, B, C, and D of Eqs. (26) are absorbed into the constants β_k and we therefore need to solve for these values of β_k. Note that in Eq. (30) the λ_k's satisfy $\mathrm{Re}(\lambda_{k+1}) > \mathrm{Re}(\lambda_k)$ and $\mathrm{Re}(\lambda_1) > 0$. Let M be such that $\mathrm{Re}(\lambda_M) < 3$ but $\mathrm{Re}(\lambda_{M+1}) \geqslant 3$. Defining functions g and χ by

$$g(r,\theta) \equiv 1 + \sum_{k=1}^{M} \beta_k r^{\lambda_k+1} f_{\lambda_k}(\theta), \tag{31}$$

$$\psi = \chi + g, \tag{32}$$

implies that χ is a biharmonic function containing no singularities up to fourth derivatives. Moreover, Eqs. (31) and (32) imply that $\chi \to 0$ and that χ', $\nabla^2\chi$, and $\nabla^2\chi'$ are bounded as $r \to 0$.

Define the function h by

$$\nabla^2\chi = h, \tag{33}$$

where, from Eq. (32),

$$h = \phi - \nabla^2 g.$$

Then, from Eq. (33)

$$\nabla^2 h = 0, \tag{34}$$

because χ is biharmonic.

So we have replaced the system of Eqs. (2) and (3) by Eqs. (33) and (34) for the biharmonic function χ whose derivatives remain bounded everywhere up to fourth order. Using arguments analogous to those already presented we have the system

$$A\boldsymbol{\chi} + B\boldsymbol{\chi}' + C\mathbf{h} + D\mathbf{h}' = 0, \tag{35}$$

$$A\mathbf{h} + B\mathbf{h}' = 0, \tag{36}$$

where now

$$\boldsymbol{\chi} = \boldsymbol{\psi} - \mathbf{g}, \tag{37a}$$

$$\boldsymbol{\chi}' = \boldsymbol{\psi}' - \mathbf{g}', \tag{37b}$$

$$\mathbf{h} = \boldsymbol{\phi} - \nabla^2 \mathbf{g}, \tag{37c}$$

$$\mathbf{h}' = \boldsymbol{\phi}' - \nabla^2 \mathbf{g}', \tag{37d}$$

where, for example,

$$\mathbf{g} = (g_1, \ldots, g_N)^T = (g(r_1, \theta_1), \ldots, g(r_N, \theta_N))^T, \tag{38}$$

and (r_i, θ_i) are the polar coordinates of boundary node q_i, $i = 1, \ldots, N$. Using Eqs. (28), (29), and (31), the analytic form of $g(r, \theta)$ in this problem is given by

$$g(r, \theta) = 1 + \beta_1 r^{3/2} \left(\cos \frac{3\theta}{2} - \cos \frac{\theta}{2}\right) + \beta_2 r^{5/2} \left(\cos \frac{5\theta}{2} - \cos \frac{\theta}{2}\right)$$

$$+ \beta_3 r^3 (\sin 3\theta - 3 \sin \theta) + \beta_4 r^{7/2} \left(\cos \frac{7\theta}{2} - \cos \frac{3\theta}{2}\right), \tag{39}$$

hence we can evaluate analytically g_i, $\nabla^2 g_i$, $\partial g_i/\partial x$, and $\partial g_i/\partial y$ for each $i = 1, \ldots, N$. Since we know any two of ψ_i, ψ_i', ϕ_i and ϕ_i' on each boundary segment $\partial\Omega_i$, then Eqs. (37) provide us with any two of χ_i, χ_i', h_i and h_i' on each segment $\partial\Omega_i$. Recalling that these "known" boundary conditions are in terms of β_1, β_2, β_3 and β_4, we have $2N + 4$ unknowns and only $2N$ equations from Eqs. (33) and (34).

Let us now look at the region near S, see Fig. 3, in more detail. If S is the common endpoint of boundary segments $\partial\Omega_s$ and $\partial\Omega_{s-1}$, then on $\partial\Omega_{s-2}$ and $\partial\Omega_{s-1}$ we have χ and h prescribed, whereas on $\partial\Omega_s$ and $\partial\Omega_{s+1}$, χ and χ' are prescribed. It has already been postulated that $\chi \to 0$ as $r \to 0$, i.e., that ψ may be represented accurately by g near S. Differentiating repeatedly we now postulate the ϕ' may be accurately represented by $\nabla^2 g'$ near S. Then Eq. (37d) implies that $h' \sim 0$ near S. In order to reduce our number of unknowns to $2N$, we specify

$$h'_{s-2} = h'_{s-1} = h'_s = h'_{s+1} = 0. \tag{40}$$

We now proceed to solve Eqs. (35) and (36) subject to Eqs. (37) and (39) with conditions (40) in precisely the same way as outlined for the solution of Eqs. (12) and (13). At this point we know $\beta_1, \beta_2, \beta_3$ and β_4 and hence use Eq. (39) to evaluate g_p at any field point $p(r, \theta) \in \Omega + \partial\Omega$. The boundary information χ, χ', $\mathbf{h}$, and $\mathbf{h}'$ is also known and using discretized relations analogous to Eqs. (4) and (5) we evaluate χ_p and h_p at that same point p. Then the MBBIE gives

$$\psi_p = \chi_p + g_p, \qquad \phi_p = h_p + \nabla^2 g_p,$$

for the stream function and vorticity at p.

3. Results

Evaluating the kernel integrals analytically rather than by Gaussian quadrature resulted in computer time savings of up to 38%.

Table I shows the stream function generated by the BBIE in the region $-3 \leqslant x \leqslant 3$, $0 \leqslant y \leqslant 1$ for eighty-one equally spaced field points in the solution domain. At each point, results are shown for discretizations of 70, 140, and 280 uniformly spaced boundary nodes. Note that results converge rapidly everywhere except near S (this includes the entire central column of figures). The errors at the corners of the solution domain are a direct result of the Maximum Principle [2] and are inherent in the BIE solution of contained harmonic and biharmonic problems. Table II shows an equivalent distribution of results for the stream function generated by the MBBIE. This table illustrates the convergence of the solution throughout the entire domain. Thus the inclusion of the analytic form of the singularity S has appreciably improved the rate of convergence of the solution.

To see the effect of the modification of the BBIE we expand the region near S and present in Tables III and IV results from the BBIE and MBBIE, respectively, in the region $-0.1 \leqslant x \leqslant 0.1$, $0.9 \leqslant y \leqslant 1.0$. Table III displays the nature of the relatively poor BBIE convergence in this region. However, Table IV shows the excellent convergence properties of the MBBIE near S; with a discretization of only 70 nodes the solution is only .01% in error near S. Figure 4 shows the streamlines $\psi =$ constant near the singularity in the regions covered by Tables III and IV. The streamlines are generated using the boundary information generated by the 280 node discretization, and show clearly the spurious effects of the BBIE near S; note in particular the erroneous $\psi = 1$ streamline from the BBIE.

In Table IV we present the values of $\beta_1, \ldots, \beta_4$ produced by different discretizations of the MBBIE. Because the nodes were uniformly distributed in each case—each boundary segment was of length h—and since the segment length was halved in each discretization, then Richardson's extrapolation to the limit [28] was applied to the values of β_1 to give $\hat{\beta}_1$, say. Now $\hat{\beta}_1$ is given analytically by the Wiener–Hopf technique [13] as

$$\hat{\beta}_1 = \frac{1}{2}\left(\frac{6}{\pi}\right)^{1/2} \sim 0.690988\ldots,$$

TABLE I

Stream Function from BBIE in $-3 \leqslant x \leqslant 3$, $0 \leqslant y \leqslant 1$

S

0.9998	1.0006	0.9994	0.9990	0.9984	0.9994	1.0000	1.0000	1.0138
0.9990	0.9999	0.9998	0.9999	0.9994	1.0000	1.0000	1.0000	1.0074
0.9986	1.0000	1.0000	1.0000	0.9998	1.0000	1.0000	1.0000	1.0041
0.9777	0.9771	0.9770	0.9767	0.9438	0.8858	0.8765	0.8750	0.8744
0.9775	0.9777	0.9775	0.9771	0.9492	0.8866	0.8766	0.8750	0.8749
0.9775	0.9780	0.9776	0.9772	0.9522	0.8871	0.8767	0.8749	0.8750
0.9141	0.9140	0.9136	0.9122	0.8580	0.7697	0.7528	0.7501	0.7496
0.9141	0.9145	0.9141	0.9127	0.8644	0.7711	0.7530	0.7500	0.7500
0.9141	0.9149	0.9142	0.9128	0.8678	0.7720	0.7531	0.7499	0.7500
0.8155	0.8158	0.8152	0.8122	0.7485	0.6503	0.6286	0.6251	0.6256
0.8154	0.8161	0.8155	0.8128	0.7547	0.6522	0.6289	0.6251	0.6250
0.8154	0.8166	0.8157	0.8131	0.7579	0.6533	0.6290	0.6249	0.6250
0.6876	0.6883	0.6874	0.6833	0.6203	0.5270	0.5039	0.5002	0.5000
0.6875	0.6884	0.6876	0.6840	0.6257	0.5289	0.5042	0.5001	0.5000
0.6875	0.6888	0.6878	0.6843	0.6285	0.5301	0.5044	0.4999	0.5000
0.5353	0.5372	0.5362	0.5319	0.4777	0.3995	0.3786	0.3753	0.3753
0.5361	0.5370	0.5362	0.5324	0.4819	0.4013	0.3789	0.3752	0.3750
0.5361	0.5374	0.5364	0.5327	0.4841	0.4023	0.3790	0.3749	0.3750
0.3677	0.3682	0.3674	0.3638	0.3244	0.2686	0.2528	0.2503	0.2498
0.3673	0.3680	0.3673	0.3641	0.3272	0.2699	0.2530	0.2502	0.2500
0.3672	0.3682	0.3674	0.3643	0.3287	0.2706	0.2531	0.2499	0.2500
0.1875	0.1874	0.1869	0.1849	0.1641	0.1350	0.1265	0.1252	0.1244
0.1867	0.1870	0.1866	0.1848	0.1654	0.1357	0.1266	0.1251	0.1249
0.1866	0.1871	0.1866	0.1849	0.1662	0.1361	0.1267	0.1250	0.1250
-0.0219	0.0011	0.0006	-0.0004	0.0008	-0.0003	0.0000	0.0000	-0.0126
-0.0119	0.0001	0.0002	0.0001	0.0001	0.0000	0.0000	0.0000	-0.0062
-0.0067	0.0000	0.0000	0.0000	0.0000	0.0000	0.0000	0.0000	-0.0027

Nodes
70
140
280

and from Table V we have

$$\hat{\beta}_1 = 0.69108.$$

Hence the MBBIE gives the dominant coefficient in the singularity expansion to an accuracy of $O(10^{-2}\%)$. However, Richardson [14] obtains a value of 0.581 for $\hat{\beta}_1$. As is usual in these types of extrapolation, the smaller the value of k the faster the β_k's converge. This phenomenon is displayed in Table V.

In the region near S, Eq. (39) gives

$$\psi \sim 1 - 2\beta_1 r^{3/2} \sin\frac{\theta}{2} \sin\theta - 2\beta_2 r^{5/2} \sin\frac{3\theta}{2} \sin\theta + O(r^3).$$

TABLE II

Stream Function from MBBIE in $-3 \leqslant x \leqslant 3, 0 \leqslant y \leqslant 1$

S

0.9945	1.0001	0.9999	0.9999	1.0001	0.9993	1.0001	1.0036	1.0262
0.9977	1.0000	1.0000	1.0000	1.0000	1.0000	1.0001	1.0000	1.0157
0.9988	1.0000	1.0000	1.0000	1.0000	1.0000	1.0000	1.0000	1.0073
0.9775	0.9785	0.9780	0.9776	0.9555	0.8876	0.8766	0.8739	0.8761
0.9775	0.9781	0.9779	0.9775	0.9555	0.8877	0.8767	0.8744	0.8739
0.9775	0.9780	0.9778	0.9774	0.9555	0.8877	0.8767	0.8745	0.8749
0.9136	0.9159	0.9150	0.9136	0.8717	0.7730	0.7528	0.7478	0.7446
0.9141	0.9152	0.9146	0.9134	0.8716	0.7731	0.7531	0.7488	0.7499
0.9141	0.9149	0.9145	0.9133	0.8716	0.7731	0.7531	0.7491	0.7500
0.8158	0.8179	0.8166	0.8141	0.7618	0.6545	0.6285	0.6221	0.6315
0.8155	0.8168	0.8161	0.8138	0.7617	0.6547	0.6290	0.6235	0.6259
0.8154	0.8166	0.8160	0.8137	0.7617	0.6547	0.6291	0.6239	0.6250
0.6874	0.6901	0.6887	0.6854	0.6320	0.5312	0.5037	0.4969	0.4998
0.6875	0.6890	0.6882	0.6851	0.6319	0.5315	0.5043	0.4985	0.5000
0.6875	0.6887	0.6881	0.6850	0.6319	0.5316	0.5044	0.4988	0.5000
0.5358	0.5386	0.5372	0.5337	0.4868	0.4032	0.3783	0.3720	0.3689
0.5360	0.5376	0.5367	0.5334	0.4868	0.4036	0.3789	0.3736	0.3741
0.5361	0.5372	0.5366	0.5333	0.4868	0.4036	0.3791	0.3739	0.3750
0.3675	0.3691	0.3680	0.3651	0.3306	0.2710	0.2522	0.2474	0.2548
0.3672	0.3683	0.3676	0.3649	0.3306	0.2715	0.2530	0.2489	0.2500
0.3672	0.3680	0.3675	0.3648	0.3306	0.2716	0.2531	0.2492	0.2500
0.1850	0.1873	0.1870	0.1855	0.1669	0.1362	0.1259	0.1220	0.1218
0.1865	0.1871	0.1868	0.1852	0.1671	0.1365	0.1265	0.1243	0.1260
0.1865	0.1870	0.1867	0.1852	0.1671	0.1366	0.1267	0.1245	0.1250
-0.0208	-0.0013	0.0002	0.0005	0.0001	0.0005	-0.0001	-0.0032	-0.0335
-0.0065	0.0000	0.0000	0.0000	0.0000	0.0000	-0.0001	0.0000	-0.0180
-0.0006	0.0000	0.0000	0.0000	0.0000	0.0000	0.0000	0.0000	-0.0081

Nodes
70
140
280

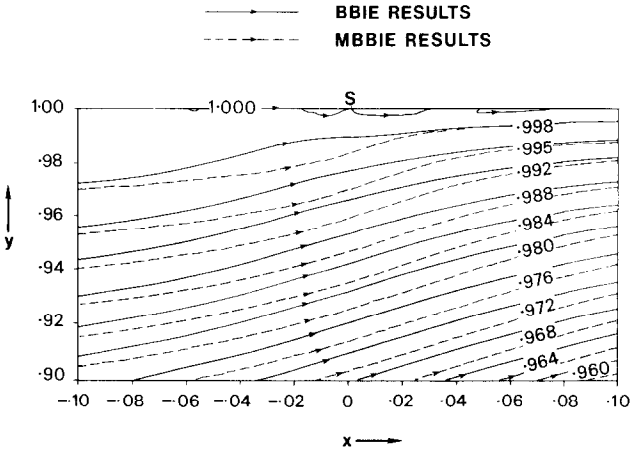

FIG. 4. A comparison of streamlines $\psi =$ constant near the singularity.

TABLE III

Stream Function from BBIE in $-0.1 \leqslant x \leqslant 0.1$, $0.9 \leqslant y \leqslant 1.0$

S

0.9949	0.9982	1.0039	1.0135	0.9984	1.0062	1.0075	1.0061	1.0032
0.9980	0.9973	0.9980	1.0018	0.9994	1.0029	1.0013	0.9975	1.0013
0.9999	0.9998	0.9992	0.9992	0.9998	1.0005	1.0006	1.0001	1.0001
0.9940	0.9932	0.9929	0.9933	0.9953	0.9972	0.9976	0.9971	0.9962
0.9984	0.9978	0.9970	0.9964	0.9966	0.9968	0.9961	0.9952	0.9945
0.9995	0.9993	0.9989	0.9981	0.9975	0.9967	0.9958	0.9950	0.9943
0.9922	0.9912	0.9905	0.9903	0.9910	0.9915	0.9913	0.9904	0.9892
0.9970	0.9961	0.9950	0.9939	0.9931	0.9922	0.9909	0.9895	0.9883
0.9983	0.9979	0.9971	0.9959	0.9944	0.9927	0.9911	0.9897	0.9886
0.9897	0.9885	0.9874	0.9866	0.9863	0.9858	0.9850	0.9837	0.9822
0.9948	0.9936	0.9922	0.9906	0.9890	0.9873	0.9855	0.9837	0.9821
0.9962	0.9956	0.9944	0.9928	0.9907	0.9885	0.9863	0.9844	0.9827
0.9866	0.9851	0.9836	0.9823	0.9812	0.9800	0.9786	0.9770	0.9752
0.9919	0.9904	0.9887	0.9867	0.9845	0.9823	0.9800	0.9778	0.9757
0.9935	0.9925	0.9911	0.9891	0.9866	0.9839	0.9812	0.9788	0.9767
0.9829	0.9811	0.9793	0.9775	0.9758	0.9741	0.9722	0.9701	0.9680
0.9883	0.9866	0.9845	0.9822	0.9796	0.9769	0.9742	0.9716	0.9692
0.9901	0.9888	0.9870	0.9847	0.9819	0.9788	0.9758	0.9730	0.9705
0.9786	0.9765	0.9744	0.9722	0.9701	0.9678	0.9655	0.9631	0.9607
0.9841	0.9822	0.9799	0.9772	0.9743	0.9712	0.9682	0.9653	0.9625
0.9860	0.9845	0.9824	0.9798	0.9768	0.9735	0.9701	0.9670	0.9641
0.9738	0.9715	0.9690	0.9665	0.9640	0.9614	0.9587	0.9560	0.9533
0.9794	0.9773	0.9747	0.9717	0.9686	0.9652	0.9619	0.9587	0.9556
0.9815	0.9796	0.9773	0.9745	0.9712	0.9677	0.9641	0.9607	0.9575
0.9685	0.9659	0.9632	0.9604	0.9576	0.9546	0.9516	0.9487	0.9457
0.9742	0.9718	0.9690	0.9659	0.9625	0.9589	0.9553	0.9518	0.9485
0.9764	0.9743	0.9717	0.9687	0.9652	0.9615	0.9578	0.9541	0.9506

Nodes
70
140
280

Then in $x > 0$ on $y = 1$,

$$\psi' = \frac{1}{r}\frac{\partial \psi}{\partial \theta}\bigg|_{r=x,\,\theta=\pi} = 2\beta_1 x^{1/2} - 2\beta_2 x^{3/2} + O(x^2),$$

so that

$$\frac{\psi'}{x^{1/2}} = 2\beta_1 - 2\beta_2 x + O(x^{3/2}). \tag{41}$$

Plotting $\psi'/x^{1/2}$ vs x (where ψ' is generated by the BBIE should therefore give a curve which coincides approximately with the straight line whose intercept and gradient are $2\beta_1$ and $-2\beta_2$, respectively, where β_1 and β_2 are generated by the MBBIE. Figure 5 shows the variation of $\psi'/x^{1/2}$ with x for both the BBIE and

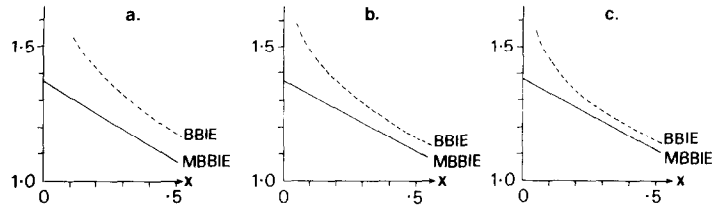

FIG. 5. A comparison of boundary information in the region $x > 0$ on $y = 1$ with 70, 140, and 280 nodes, respectively, (a)–(c). $(\cdots)\psi'/\sqrt{x}$ from BBIE, $(—)2\beta_1 - 2\beta_2 x$ from MBBIE.

TABLE IV

Stream Function from MBBIE in $-0.1 \leqslant x \leqslant 0.1$, $0.9 \leqslant y \leqslant 1.0$

S

1.0000	1.0000	1.0000	1.0000	1.0001	1.0001	1.0001	1.0001	1.0000
1.0000	1.0000	1.0000	1.0000	1.0000	1.0000	1.0000	1.0000	1.0000
1.0000	1.0000	1.0000	1.0000	1.0000	1.0000	1.0000	1.0000	1.0000
0.9996	0.9996	0.9995	0.9993	0.9987	0.9973	0.9962	0.9954	0.9947
0.9996	0.9996	0.9995	0.9993	0.9986	0.9972	0.9962	0.9954	0.9947
0.9996	0.9996	0.9995	0.9993	0.9986	0.9972	0.9962	0.9954	0.9947
0.9985	0.9984	0.9981	0.9975	0.9961	0.9941	0.9922	0.9907	0.9894
0.9985	0.9983	0.9980	0.9975	0.9961	0.9941	0.9922	0.9907	0.9894
0.9985	0.9983	0.9980	0.9975	0.9961	0.9940	0.9922	0.9907	0.9894
0.9967	0.9963	0.9957	0.9947	0.9929	0.9904	0.9880	0.9858	0.9840
0.9967	0.9963	0.9957	0.9947	0.9928	0.9904	0.9879	0.9858	0.9840
0.9967	0.9963	0.9957	0.9947	0.9928	0.9904	0.9879	0.9858	0.9840
0.9942	0.9936	0.9926	0.9912	0.9890	0.9862	0.9833	0.9807	0.9783
0.9941	0.9935	0.9926	0.9911	0.9889	0.9861	0.9833	0.9807	0.9783
0.9941	0.9935	0.9926	0.9911	0.9889	0.9861	0.9833	0.9807	0.9783
0.9910	0.9901	0.9889	0.9870	0.9845	0.9815	0.9783	0.9753	0.9725
0.9910	0.9901	0.9888	0.9870	0.9845	0.9814	0.9783	0.9752	0.9725
0.9909	0.9901	0.9888	0.9870	0.9845	0.9814	0.9782	0.9752	0.9725
0.9872	0.9861	0.9845	0.9824	0.9796	0.9763	0.9729	0.9695	0.9664
0.9872	0.9860	0.9844	0.9823	0.9795	0.9763	0.9728	0.9695	0.9664
0.9871	0.9860	0.9844	0.9823	0.9795	0.9763	0.9728	0.9695	0.9664
0.9829	0.9815	0.9796	0.9772	0.9742	0.9707	0.9671	0.9635	0.9601
0.9828	0.9814	0.9795	0.9771	0.9741	0.9707	0.9671	0.9635	0.9600
0.9828	0.9814	0.9795	0.9771	0.9741	0.9707	0.9670	0.9635	0.9600
0.9780	0.9763	0.9742	0.9716	0.9684	0.9648	0.9609	0.9571	0.9535
0.9779	0.9762	0.9741	0.9715	0.9683	0.9647	0.9609	0.9571	0.9534
0.9779	0.9762	0.9741	0.9715	0.9683	0.9647	0.9609	0.9571	0.9534

Nodes
70
140
280

TABLE V

Variation of Singularity Expansion Coefficients for Different MBBIE Discretizations

Nodes	Boundary Segment Length, h	β_1	β_2	β_3	β_4
70	0.20	0.68701	0.29559	−0.09985	−0.05625
140	0.10	0.69024	0.27706	−0.09119	−0.03452
280	0.05	0.69091	0.26952	−0.08629	−0.01725
Extrapolation to the limit		0.69108	0.26435	−0.07990	+0.04962

MBBIE. Using the BBIE it is seen that $\psi'/x^{1/2} \to \infty$ as $x \to 0^+$. This is because the values of $\nabla^2\psi$ and $\nabla^2\psi'$ in the BBIE become unbounded as we approach S along $y = 1$ in $x > 0$, and the inaccuracies incurred in these values propagate into the solution for ψ and ψ' during the matrix inversion described earlier. However, for $x > 0.1$ on $y = 1$, the agreement predicted by Eq. (41) is seen to be good and moreover it improves as the boundary discretization is refined.

From Eqs. (22) and (41) we have the x component of velocity on $y = 1$ given by

$$u(x, 1) = \frac{\partial \psi}{\partial y}\bigg|_{y=1} = \psi' = 2\beta_1 x^{1/2} + O(x^{3/2}). \tag{42}$$

Watson [13], using the Wiener–Hopf technique, obtained

$$u(x, 1) \sim \left(\frac{6x}{\pi}\right)^{1/2} \sim 1.382x^{1/2} \qquad \text{as } x \to 0^+, \tag{43}$$

whereas the MBBIE, using the extrapolated value of β_1 in expression (42), gives

$$u(x, 1) \sim 2\hat{\beta}_1 x^{1/2} \sim 1.382x^{1/2} \qquad \text{as } x \to 0^+. \tag{44}$$

However, Richardson's [14] analytic methods produced the result

$$u(x, 1) \sim \frac{3}{\pi\{\Gamma(5/4)\}^2} x^{1/2} \sim 1.162x^{1/2} \qquad \text{as } x \to 0^+. \tag{45}$$

Since the MBBIE and the analytic results of Watson [13] agree to an accuracy of order $10^{-2}\%$ it suggests that the Richardson [14] result is questionable.

Evaluation of p_c, the fluid pressure on the centreline $y = 0$, is readily accomplished by the BBIE using the boundary information already generated. From the equation for the dimensionless pressure

$$\nabla p = \nabla^2 \mathbf{u},$$

we have

$$\frac{\partial p_c}{\partial x} = \nabla^2 u|_{y=0}. \tag{46}$$

Using the commutativity of operators in Cartesian coordinates, on $y = 0$ we have

$$\nabla^2 u = \nabla^2 \left(\frac{\partial \psi}{\partial y}\right) = \frac{\partial}{\partial y}(\nabla^2 \psi) = \frac{\partial \phi}{\partial y} = -\phi', \tag{47}$$

where ϕ is as defined in Eqs. (2) and (3). Since we know ϕ_j', $j = 1,..., N$, from the BBIE, then Eqs. (46) and (47) give

$$\frac{\partial p_c}{\partial x} + \phi' = 0,$$

which was integrated by the central difference scheme

$$p_{j+1} = p_{j-1} - 2h\phi_j', \tag{48}$$

where h is as shown in Fig. 1 and $p_j \equiv p(x_j)$. Equation (48) should be integrated by applying the condition $p \to 0$ as $x \to +\infty$. In practice, it was integrated by applying $p = 0$ at $x = +3$. The pressure p_c evaluated using (48) is plotted in Fig. 6, and this compares well with the centreline pressure derived by Richardson [14]. From Fig. 6 the pressure for large negative x behaves as

$$p_c \sim -3x + p_0, \tag{49}$$

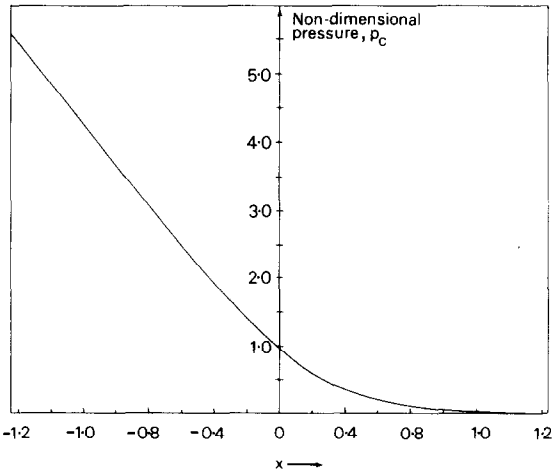

FIG. 6. Pressure variation along the centreline $y = 0$.

where p_0 is a constant. The entry length l is defined as the value of x where the straight line given by Eq. (49) cuts the x axis. If p_N and l_N represent respectively the pressure in $x < 0$ and entry length from the BBIE with N nodes, we find from numerical integration of Eq. (48) that

$$p_{70} = -3.0154x + 0.6215, \tag{50a}$$

$$p_{140} = -3.0098x + 0.7274, \tag{50b}$$

$$p_{280} = -3.0030x + 0.7858, \tag{50c}$$

which, on putting $p_N = 0$ gives

$$l_{70} = 0.2061, \tag{51a}$$

$$l_{140} = 0.2417, \tag{51b}$$

$$l_{280} = 0.2617. \tag{51c}$$

Using Richardson's Extrapolation to the limit, Eqs. (51) give

$$\hat{l} = \lim_{N \to \infty} l_N = 0.2873.$$

Watson [13] finds that the entry length is given by

$$l = \frac{1}{\pi} - \frac{1}{\pi} \int_0^\infty \frac{t \sinh t + t^2 - 4 \cosh t + 4}{t(\cosh t - 1)(\sinh t - t)} dt.$$

Numerical calculation of this integral leads to the value

$$l = 0.2865.$$

Thus the entry length generated by the BBIE is in error from the value predicted by Watson [13] by less than 1%.

In order to compare our numerical results with those of Coleman [12] we first note that he employs the boundary conditions

$$u = 1 - y^2, \qquad v = 0 \qquad \text{on } x = -2,$$

$$u = \tfrac{2}{3}, \qquad v = 0 \qquad \text{on } x = +2,$$

thus his computations are carried out on a smaller solution domain than ours. In order to compare velocities between the methods used in this paper and Coleman's [12] we first scale up his velocities by a factor of $\frac{3}{2}$. Using an argument analogous to that employed in deriving Eq. (41) and recalling Eq. (32), we have

$$u(x_j, 1) \sim 2x_j^{1/2} \{\beta_1 - \beta_2 x_j + \beta_4 x_j^2\} + \chi_j', \tag{52}$$

giving us the MBBIE x component of velocity at node x_j on $y = 1$. The BBIE x component of velocity is given by

$$u(x_j, 1) = \psi'_j. \tag{53}$$

Table VI shows a comparison of values of $u(x_j, 1)$ as obtained by Coleman [12], the BBIE, and the MBBIE using the same boundary discretization. Furthermore, the results presented in the MBBIE column are almost indistinguishable from the those which are obtained using four times as many nodes. It is seen that both Coleman [12] and the BBIE are over 20% in error near the singularity, but for $x \geqslant 0.1$ the Coleman [12] results and the BBIE differ from the MBBIE by less than 3%.

TABLE VI

Variation of $u(x_j, 1)$ for Three Different Methods

	$10^4 u(x_j, 1)$		
$30x_j$	Coleman [12]	BBIE	MBBIE
1	2940	3751	2493
3	4610	4636	4208
5	5600	5654	5293
7	6340	6382	6102
9	6940	6970	6741
11	7420	7452	7260
13	7830	7853	7690
15	8160	8188	8049
17	8450	8472	8351
19	8690	8711	8607
21	8880	8914	8823
23	9060	9087	9007
25	9200	9234	9163
27	9330	9359	9296
29	9420	9465	9409
31	9510	9556	9505
33	9590	9633	9587
35	9640	9699	9659
37	9700	9756	9718
39	9750	9805	9770
41	9790	9848	9815
43	9820	9885	9854
45	9840	9919	9889
47	9870	9949	9920
49	9890	9977	9949
51	9900	10044	9977

4. Conclusions

By using a coupled form of the biharmonic equation a direct BBIE method has been formulated. Employment of analytically evaluated integrals means that this BBIE is more efficient than previously formulated BBIEs in that program-execution time savings of up to 38% over numerical quadrature have been observed. The actual saving is dependent upon the size of the discretization and increases as the number of nodes increases. Furthermore, for each discretization the MBBIE program required approximately 5% more execution time than the corresponding BBIE program, so that the accuracy of the solution was noticeably improved without appreciably lengthening the method.

Testing the method on the classical "stick–slip" problem has shown that the BBIE produces accurate results. The BBIE and MBBIE formulated here are stable for any linear boundary conditions and use but one Gaussian elimination matrix inversion for solution and so are computationally efficient.

Here the analytic nature of the singularity has been incorporated into the MBBIE to avoid the problem of unbounded derivatives occurring in the solution domain. Results indicate substantial improvements in the accuracy of the solution near the singularity when the MBBIE is employed.

This MBBIE can be applied to problems involving more complex geometries and boundary conditions, with the result that the forms of singularity encountered will be correspondingly more complex. In fact, it can be applied to any problem for which the analytic form of the singularity can be obtained.

Acknowledgments

I wish to express my thanks to Dr. D. B. Ingham for his guidance and numerous helpful suggestions. My thanks are also due to the Science and Engineering Research Council for the provision of a grant. All numerical work was performed on the AMDAHL 470 system at the University of Leeds.

References

1. S. K. Laskar, Ph. D. Thesis, University College London, 1971.
2. M. A. Jaswon and G. T. Symm, "Integral Equation Methods in Potential Theory and Elastostatics," Academic Press, New York/London, 1977.
3. C. A. Brebbia (Ed.). "Recent Advances in Boundary Element Methods," Pentech, London, 1978.
4. P. K. Banerjee and R. Butterfield, "Development in Boundary Element Methods No. 1," Applied Science, Essex, 1981.
5. C. W. Miller, Ph. D. Thesis, University of Iowa, Iowa City, 1979.
6. G. K. Youngren and A. Acrivos, *J. Fluid Mech.* **69** (2) (1975), 377.
7. G. K. Youngren and A. Acrivos, *J. Fluid Mech.* **76** (3) (1976), 433.
8. J. M. Rallison and A. Acrivos, *J. Fluid Mech.* **89** (1) (1978), 191.
9. J. M. Rallison, *J. Fluid Mech.* **109** (1981), 465.
10. A. Mir–Mohamed–Sadegh and K. R. Rajagopal, *Trans. ASME Ser. E J. Appl. Mech.* **47** (3) (1980), 485.

11. J. R. BLACK, M. M. DENN, AND G. C. HSIAO, *in* "Theoretical Rheology" (J. F. Hutton, J. R. A. Pearson, and *K.* Walters, Eds.), pp. 3–30, Halsted, New York, 1975.
12. C. J. COLEMAN, *Q. J. Mech. Appl. Math.* **34** (4) (1981), 453.
13. E. WATSON, private communication, 1981.
14. S. RICHARDSON, *Proc. Cambridge Philos. Soc.* **67** (1970), 477.
15. H. MOTZ, *Q. Appl. Math.* **4** (4) (1946), 371.
16. G. T. SYMM, National Physics Laboratory Report, No. NAC31, 1973.
17. D. B. INGHAM, P. J. HEGGS, AND M. MANZOOR, *IEEE Trans. Microwave Theory Tech.* **MTT-29** (1981), 1240.
18. D. B. INGHAM, P. J. HEGGS, AND M. MANZOOR, *J. Comput. Phys.* **42** (1), (1981), 77.
19. L. S. XANTHIS, M. J. M. BERNEL, AND C. ATKINSON, *Comput. Methods Appl. Mech. Eng.* **26** (3) (1981), 285.
20. O. R. BURGGRAF, *J. Fluid Mech.* **24** (1) (1966), 113.
21. F. PAN AND A. ACRIVOS, *J. Fluid Mech.* **28** (4) (1967), 643.
22. D. H. MICHAEL, *Mathematika* **5** (1958), 82.
23. G. FAIRWEATHER, F. J. RIZZO, D. J. SHIPPY, AND Y. S. WU, *J. Comput. Phys.* **31** (1) (1979), 96.
24. M. MAITI AND S. K. CHAKRABARTY, *Int. J. Eng.* **12** (1974), 793.
25. Y. S. WU, F. J. RIZZO, D. J. SHIPPY, AND J. A. WAGNER, *Q. Elec. Mach. Electromech.* 1 (1977), 301.
26. H. K. MOFFATT, *J. Fluid Mech.* **18** (1) (1964), 1.
27. W. R. DEAN AND P. E. MONTAGNON, *Proc. Cambridge Philos Soc.* **45** (1949), 389.
28. G. D. SMITH, "Numerical Solution of Partial Differential Equations: Finite Difference Methods," Oxford Univ. Press (Clarendon), London/New York, 1978.